Comparing EMG-Based Human-Machine Interfaces for Estimating Continuous, Coordinated Movements

Lizhi Pan, *Member, IEEE*, Dustin L. Crouch, and He Huang, *Senior Member, IEEE*

***Abstract*— Electromyography (EMG)-based interfaces are trending toward continuous, simultaneous control with multiple degrees of freedom. Emerging methods range from data-driven approaches to biomechanical model-based methods. However, there has been no direct comparison between these two types of continuous EMG-based interfaces. The aim of this study was to compare a musculoskeletal model (MM) with two data-driven approaches, linear regression (LR) and artificial neural network (ANN), for predicting continuous wrist and hand motions for EMG-based interfaces. Six able-bodied subjects and one transradial amputee subject performed (missing) metacarpophalangeal (MCP) and wrist flexion/extension, simultaneously or independently, while four EMG signals were recorded from forearm muscles. To add variation to the EMG signals, the subjects repeated the MCP and wrist motions at various upper extremity postures. For each subject, the EMG signals collected from the neutral posture were used to build the EMG interfaces; the EMG signals collected from all postures were used to evaluate the interfaces. The performance of the interface was quantified by Pearson's correlation coefficient (r) and the normalized root mean square error (NRMSE) between measured and estimated joint angles. The results demonstrated that the MM predicted movements more accurately, with higher r values and lower NRMSE, than either LR or ANN. Similar results were observed in the transradial amputee. Additionally, the variation in r across postures, an indicator of reliability against posture changes, was significantly lower (better) for the MM than for either LR or ANN. Our findings suggest that incorporating musculoskeletal knowledge into EMG-based human-machine interfaces could improve the estimation of continuous, coordinated motion.**

Manuscript received February 22, 2019; revised July 1, 2019; accepted August 16, 2019. Date of publication August 27, 2019; date of current version October 8, 2019. This work was supported in part by the Defense Advanced Research Projects Agency (DARPA), Biological Technologies Office (BTO), through the Hand Proprioception and Touch Interfaces (HAPTIX) Program of the DARPA Contracts Management Office under Grant N66001-16-2-4052, in part by NSF under Grant 1527202 and Grant 1637892, and in part by the Department of Defense under Grant W81XWH-15-C-0125 and Grant W81XWH-15-1-0407. *(Corresponding author: He Huang.)*

L. Pan and H. Huang are with the UNC/NC State Joint Department of Biomedical Engineering, North Carolina State University, Raleigh, NC 27695- 7115 USA, and also with the University of North Carolina at Chapel Hill, Chapel Hill, NC 27599 USA (e-mail: lpan3@ncsu.edu; hhuang11@ncsu.edu).

D. L. Crouch was with the UNC/NC State Joint Department of Biomedical Engineering, North Carolina State University, Raleigh, NC 27695-7115 USA, also with the University of North Carolina at Chapel Hill, Chapel Hill, NC 27599 USA, and also with the Department of Mechanical, Aerospace, and Biomedical Engineering, University of Tennessee, Knoxville, TN 37996 USA (e-mail: dustin.crouch@utk.edu).

Digital Object Identifier 10.1109/TNSRE.2019.2937929

***Index Terms*— Electromyography (EMG), musculoskeletal model, linear regression, artificial neural network, comparison.**

I. Introduction

ELECTROMYOGRAPHY (EMG) signals have been widely used as control inputs for human-machine interface (HMI), such as prosthesis control [1]–[5], rehabilitation virtual reality control [6]–[9], rehabilitation device control [10]–[15], teleoperation [16]–[18], and other applications. A traditional EMG-based HMI uses the amplitude of EMG from an agonist-antagonist muscle pair to control 1 degree of freedom (DoF). However, this process requires the user to cocontract the two muscles to generate a switching command for sequential control of two or more DoFs [19], [20]. Pattern recognition-based myoelectric control has been developed to improve the functionality (i.e., switching more intuitively among DoFs) of EMG-based HMIs [9], [21]–[32]. Nevertheless, the pattern recognition-based control scheme is still nonintuitive, since it is discrete-motion control, only allowing the user to control one joint or motion class at a time.

EMG-based HMIs are trending toward continuous (or proportional), coordinated control of multiple joints at a time (hereafter referred to as continuous control). Continuous control is a hallmark of physiologic motor control [33] and, thus, may make myoelectric control more intuitive. It could also allow users to perform tasks more efficiently than they would if they could only control one joint at a time. Advanced EMG decoders based on data-driven, machine learning algorithms have been developed to estimate joint angles from surface EMG for continuous control [33]–[41]. Three continuous control algorithms are notable for their relatively high offline and real-time performance in estimating continuous movements from EMG: (1) nonnegative matrix factorization (NMF) for wrist movements [34], [37], (2) linear regression (LR) for wrist and hand movements [38]–[40], and (3) artificial neural network (ANN) for wrist and hand movements [33], [35], [36].

Recently, several research groups explored the possibility of building EMG-based continuous controllers from musculoskeletal models (MMs) [42]–[48]. The motivation for an MM-based control is that by encoding explicit representations of anatomical structures of the musculoskeletal system, it may better mimic physiologic human movement than data-driven algorithms, which are naïve to musculoskeletal anatomy. One research group developed an MM of the shoulder and the

elbow for dynamic simulation of arm movements [42], [44]. An MM that included 24 muscles crossing the wrist and fingers, and 23 DoF was proposed for real-time control [43]. An MM that included 10 muscles crossing the wrist and fingers, and 3 DoF was developed for real-time prosthesis control [47]. In our group, we recently developed an EMG HMI based on an MM for continuous control of wrist and hand movements [45], [49]. The parameters of our MM, identified through an optimization procedure using measured kinematics and EMG data [45], only need to be calculated once for each subject. Promisingly, our previous results demonstrated that the MM-based HMI could reasonably estimate joint angles offline [45] and enable effective real-time control for performing virtual tasks while mimicking the dynamics of the intact human hand [50].

As the number and variety of continuous control approaches grows, an emerging challenge is determining which approaches are most promising and worth advancing toward clinical application. Some research has been performed to compare among control approaches in order to identify promising ones. Linear and nonlinear regression algorithms were compared for continuous control of wrist movements [38]. LR, ANN, and NMF were compared for continuous control of wrist movements [51]. However, no one has compared existing data-driven continuous control approaches with an MM-based approach.

In this study, we focused on continuous myoelectric control rather than discrete control methods, such as pattern recognition-based myoelectric control. Therefore, we chose to compare our MM to LR and ANN, two of the three data-driven algorithms highlighted above that enable continuous myoelectric control. We compared performance among the three algorithms (MM, LR, and ANN) for estimating simultaneous wrist and hand movements from EMG. Because NMF is a semi-supervised approach requiring clearly identified positive and negative directions of movement in each DoF, it is not suitable for estimating hand movements from EMG signals and, therefore, was not selected for our comparison in this study. To account for EMG variability due to differences in limb posture [52]–[59], we quantified estimation performance from EMG measured across several upper limb postures. To purely study the performance of the algorithms and minimize the effect of human adaptation efforts, it was essential that we conducted a comparison of the estimation performance among those three different methods on an offline data set rather than for real-time control. We hypothesized that the estimation performance of the MM would be better than that of the LR and ANN.

II. Methods

A. Subjects

Six able-bodied (AB) subjects (male, ages 19-32, right hand dominant) and one amputee subject (male, age 42, right transradial amputation) participated in the experiment. The protocol was approved by the Institutional Review Board of the University of North Carolina at Chapel Hill. All subjects signed informed consent forms to participate. The amputee subject used both a body-powered prosthesis and a myoelectric prosthesis with direct control in daily life.

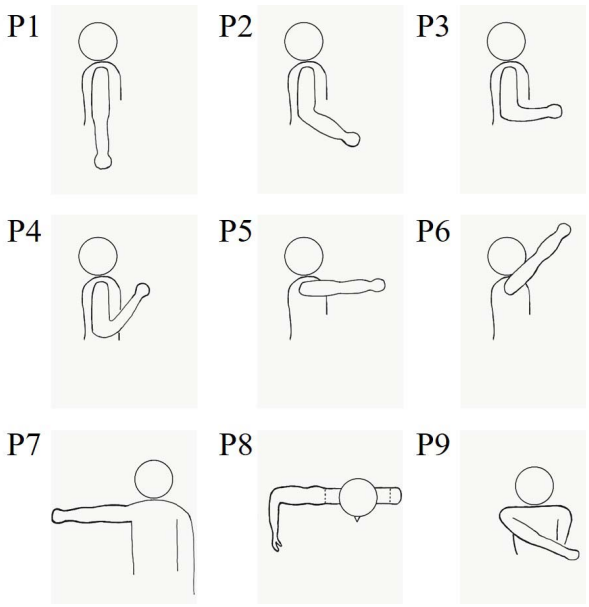

Fig. 1. The 9 different upper limb postures tested in the experiments.

B. Experiment Protocol

Kinematic and EMG data were recorded synchronously from all AB subjects in nine upper limb postures (P1-P9 in Fig. 1). The postures, covering a wide range of the upper limb workspace and different hand orientations with respect to gravity, reflected the variety of limb postures that might be assumed to perform daily living tasks. Since the amputee subject fatigued relatively quickly, EMG and kinematic data were recorded for three of the nine upper limb postures (P3, P5, and P7). In each posture, the subjects conducted five different types of movements either at a fixed speed (rhythm) or with continuously variable speed (random): (a) wrist flexion/extension (WFLX/EXT) only, rhythm; (b) metacarpophalangeal (MCP) flexion/extension (MFLX/EXT) only, rhythm; (c) WFLX/EXT only, random; (d) MFLX/EXT only, random; (e) simultaneous WFLX/EXT and MFLX/EXT, random. All AB subjects conducted the movements with the dominant limb, while the amputee subject conducted mirrored bilateral movements. In each trial, one type of movement was conducted for 20 s. Two trials were conducted for each type of movement. The subject rested for approximately one minute between each trial to avoid fatigue.

C. Data Acquisition

We computed wrist and hand kinematics from the three-dimensional positions of fourteen retro-reflective markers recorded at 120 Hz by an infrared motion capture system (Vicon Motion Systems Ltd. UK). We placed the markers over the following anatomical locations (Fig. 2a): xiphoid, acromion, C7 spinous process, medial clavicle, humeral midshaft, medial humeral epicondyle, lateral humeral epicondyle, radial midshaft, radial styloid process, ulnar styloid process,

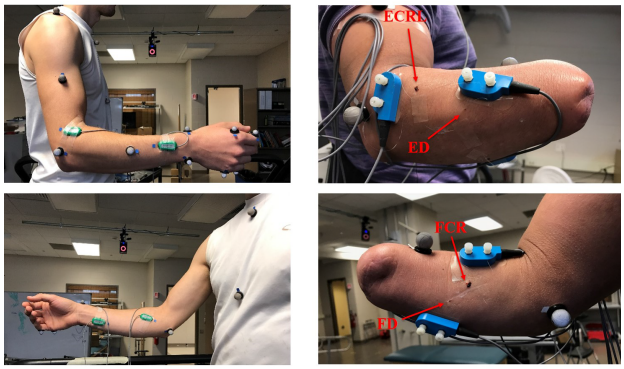

Fig. 2. Experimental setup. (a) The positions of the markers and the surface EMG electrodes on an AB subject; (b) The positions of the fine-wire EMG electrodes on the amputee subject.

2nd and 5th MCP joints, and 2nd and 5th proximal interphalangeal joints. Because the (intended) wrist and hand motion could not be determined directly from the residual limb of the amputee subject, we recorded kinematic data from the intact limb during the mirrored bilateral movements.

For all AB subjects, surface EMG signals were recorded from four muscles (Fig. 2a): extensor digitorum (ED), flexor digitorum (FD), extensor carpi radialis longus (ECRL), and flexor carpi radialis (FCR). The skin was cleaned with an alcohol pad to reduce the impedance. Four bipolar surface electrodes (SX230 W4X8, Biometrics Ltd., UK) were placed on the target muscles using medical adhesive tape. The electrodes were connected to an amplifier (K800 Amplifier, Biometrics Ltd. UK), which was connected to the analog-to-digital (AD) interface unit of the motion capture system. The surface EMG signals were recorded at 960 Hz.

For the transradial amputee, the same four muscles were targeted from the residual forearm (Fig. 2b). Identifying the muscle-specific EMG needed for the MM-based interface is difficult with surface electrodes in some transradial amputees, since muscles associated with MCP flexion and extension lie deep to muscles associated with wrist movement in the proximal residual forearm. Therefore, fine-wire electrodes were used to record EMG from the amputee subject. Under ultrasound guidance, fine-wire bipolar EMG electrodes were inserted percutaneously into the belly of the target muscles. The fine-wire electrodes were connected to an EMG system (MA300 DTU, Motion Lab Systems, USA), which was connected to the analog-to-digital (AD) interface unit of the motion capture system. The fine-wire EMG signals were also recorded at 960 Hz.

D. Data Processing

We used a modified existing upper extremity MM in OpenSim [60] to calculate upper limb joint angles. The wrist joint was modeled as a hinge joint with 1 DoF (flexion/extension), and the MCP joints of the hand were modeled as a single hinge joint with 1 DoF (flexion/extension).

The EMG were filtered using a 4th-order Butterworth high-pass filter with a cutoff frequency at 40 Hz, rectified, filtered using a 4th-order Butterworth low-pass filter with a cutoff frequency at 6 Hz, and then normalized by the maximum EMG acquired during maximum voluntary contraction. The normalized EMG were downsampled to 120 Hz and used to calculate muscle activations using a nonlinear model of excitation-activation dynamics [61], [62]. The transformation functions from the downsampled EMG to muscle activations were as follows:

$$u_i(t) = \alpha e_i(t-d) - \beta_1 u_i(t-1) - \beta_2 u_i(t-2) \quad (1)$$

$$a_i(t) = \frac{e^{Au_i(t)} - 1}{e^A - 1} \quad (2)$$

where $e_i(t)$ is the downsampled EMG of muscle i at time t, d is the electromechanical delay, $u_i(t)$ is the postprocessed EMG of muscle i at time t, α, β_1, β_2 are the coefficients defining the second order dynamics, $a_i(t)$ is the activation of muscle i at time t. A set of constraints was used to ensure a stable solution and maintain the unit gain of equation (1):

$$\beta_1 = C_1 + C_2 \quad (3)$$

$$\beta_2 = C_1 \cdot C_2 \quad (4)$$

$$|C_1| < 1 \quad (5)$$

$$|C_2| < 1 \quad (6)$$

$$\alpha - \beta_1 - \beta_2 = 1 \quad (7)$$

E. Algorithms Modeling

We defined the posture P3 as the neutral posture, as it was the upper limb posture the subjects assumed when placing EMG electrodes. For all three algorithms (MM, LR, and ANN), the experimentally derived muscle activations and the 2-DoF joint angles of the neutral posture P3 were used as the training data to optimize the parameters of the models. Data from the first half of the trials in P3 (5 trials, 6000 sample points in total for each subject), one trial for each type of movement, were used for optimization of the first half of the models. The first half of the models were then tested in the second half of the trials in 9 tested postures (45 trials, 54000 sample points in total for each subject). Data from the second half of the trials in P3 (5 trials, 6000 sample points in total for each subject), one trial for each type of movement, were used for optimization of the second model. The second half of the models were then tested in the first half of the trials in 9 tested postures (45 trials, 54000 sample points in total for each subject).

Regarding the MM, a planar lumped-parameter MM of the wrist and hand was used in the current study [45], [50]. The model included two DoFs, WFLX/EXT and MFLX/EXT. Four muscles were included in the model: one antagonist muscle pair crossing the wrist only and another antagonist muscle pair crossing both the wrist and MCP joints. This muscle arrangement was chosen for the following reasons: 1. it is similar to the arrangement of muscles that cross the biological wrist and MCP joints; 2. it permitted independent control of wrist and MCP joint movements in both directions. Each muscle was modeled as a Hill-type actuator with a contractile element and a parallel elastic element [63]. To reduce the number of model

TABLE I
CONSTRAINTS OF THE PARAMETERS OF THE MUSCULOSKELETAL MODEL

Parameter	Constraint
$L_0^{CE}(m)$	$0.01 \leq L_0^{CE} \leq 0.5$
$F_0^{CE}(N)$	$10 \leq F_0^{CE} \leq 1000$
$ma_{wrist}(m)$	$0.001 \leq ma_{wrist} \leq 0.05$
$ma_{MCP}(m)$	$0.001 \leq ma_{MCP} \leq 0.05$
$L_{\theta=0}^{CE}(none)$	$0.75L_0^{CE} \leq L_{\theta=0}^{CE} \leq 1.25L_0^{CE}$
$K^{PEE}(N/m^2)$	$10 \leq K^{PEE} \leq 200$

L_0^{CE}: Optimal contractile element length
F_0^{CE}: Maximum isometric contractile element force
ma_{wrist}: Moment arm at wrist
ma_{MCP}: Moment arm at MCP
$L_{\theta=0}^{CE}$: Contractile element length in neutral posture
K^{PEE}: Passive elastic element stiffness
$ma_{MCP} = 0$ for wrist flexor/extensor muscles

parameters, a series elastic element representing a tendon in the Hill-type model was not included. Six parameters were optimized for each muscle: maximum isometric force, muscle length at neutral position, optimal muscle length, parallel elastic element stiffness, and moment arms at the WFLX/EXT and MFLX/EXT. We set the moment arms to zero at joints in which a muscle does not cross anatomically. We constrained all parameters to the approximate ranges of physiologic values (Table 1). We assumed that all moment arms were constant across joint angles [45]. We used the optimization function GlobalSearch in MATLAB (Mathworks, MA) to calculate the muscle parameters for each subject. The muscle parameters were optimized to minimize the mean squared error between estimated and measured joint angles.

Regarding the LR modeling, one linear regression model was used for each DoF (two LR models total) to estimate joint angles from the experimentally derived muscle activations based on the selection in the previous studies [39]–[41].

$$y = a^T * x \tag{8}$$

where y was the estimated joint angle, a was the vector of coefficients for each muscle activation, and x was the vector of muscle activation for each of the four muscles. Two different LR models were used instead of one model to obtain better estimates of the two joint angles.

Regarding the ANN modeling, one three-layer network was used for each DoF (two ANN models total) to estimate joint angles from the experimentally derived muscle activations [33], [36], [38], [51]. We tested the performance of ANN while the number of neurons in the hidden layer was set from 1 to 10. Three neurons in the hidden layer achieved the best performance. Therefore, the number of neurons in the hidden layer was set to 3.

F. Evaluation Metrics and Methods

For each subject, the MM, LR, and ANN were then tested by data recorded from each of the nine tested postures. The procedures for comparing the MM, LR, and ANN are shown in Fig. 3. To quantify the performance of the algorithms

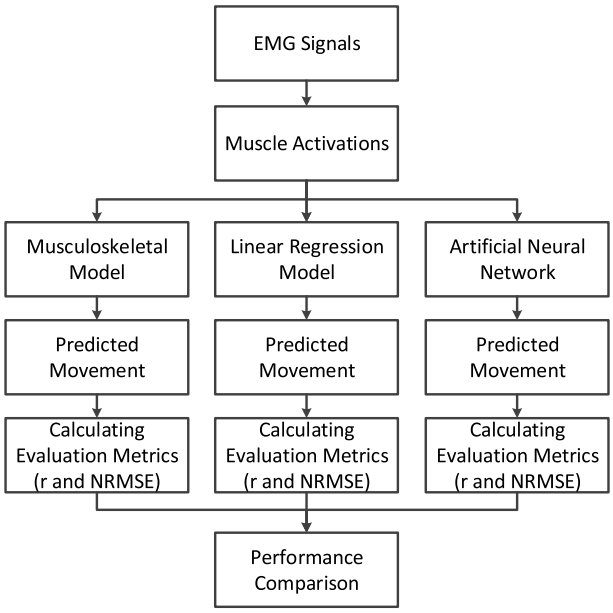

Fig. 3. Block diagram of the procedures of comparing the MM, LR, and ANN.

in each joint, we computed Pearson's correlation coefficient (r) between the measured and estimated angles for each joint.

$$r_{x,y} = \frac{\sum_1^n (x_i - \bar{x})(y_i - \bar{y})}{\sqrt{\sum_1^n (x_i - \bar{x})^2}\sqrt{\sum_1^n (y_i - \bar{y})^2}} \tag{9}$$

where x_i is the ith measured joint angle, $\bar{x}$ is the mean of measured joint angles, y_i is the ith estimated joint angle, $\bar{y}$ is the mean of estimated joint angles, and n is the number of data samples. The higher the coefficient is, the better the waveforms match between measured and estimated joint movements.

Additionally, the normalized root mean square error (NRMSE) was calculated at each joint by (1) calculating the total root mean square error (RMSE) between measured and estimated joint angles across a trial and (2) normalizing the RMSE by each subject's approximate maximum range of motion of the respective joint measured during the experiment.

$$NRMSE = \frac{\sqrt{\frac{1}{n}\sum_1^n (x_i - y_i)^2}}{(x_{\max} - x_{\min})} \tag{10}$$

where $x_{\max}$ and $x_{\min}$ are the maximum and minimum values of measured joint angles, respectively, x_i is the ith measured joint angle, y_i is the ith estimated joint angle, and n is the number of data samples. The NRMSE quantified the match of measured and estimated joint movements in both waveform and magnitude.

G. Statistical Analysis

Two-way repeated measures ANOVA was conducted on r and NRMSE. ANOVA included two independent variables: algorithm type (MM, LR, and ANN) and posture (9 different upper limb postures). One-way repeated measures ANOVA was conducted on variations in r and NRMSE across different postures, including algorithm type (MM, LR, and ANN) as

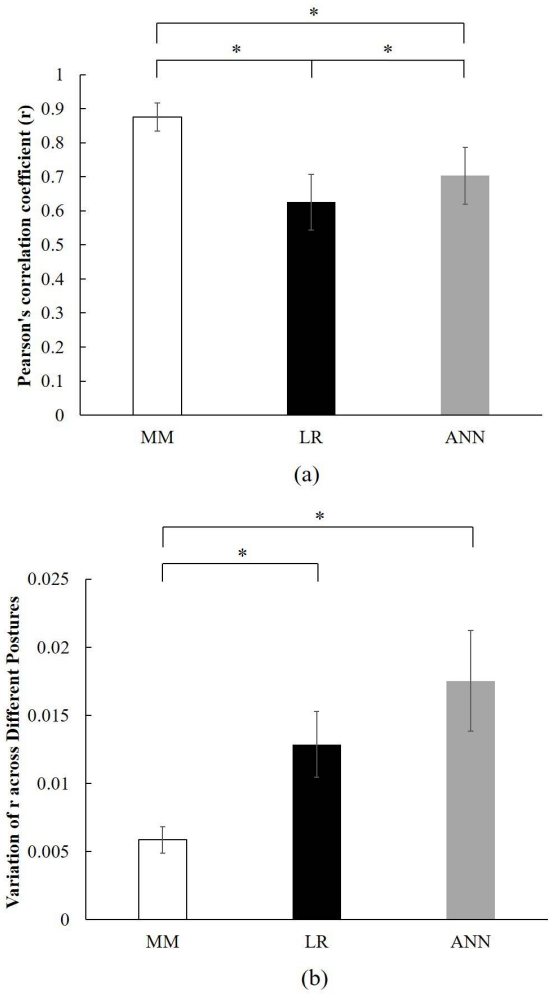

Fig. 4. (a) Pearson's correlation coefficient (r) between measured and estimated joint angles averaged across all AB subjects, movement types, joints, and postures for the test on MM (white bar), LR (black bar), and ANN (gray bar). (b) Variation in r across different postures. Tests marked by * indicate significant differences between algorithm types. Error bars represent the standard error.

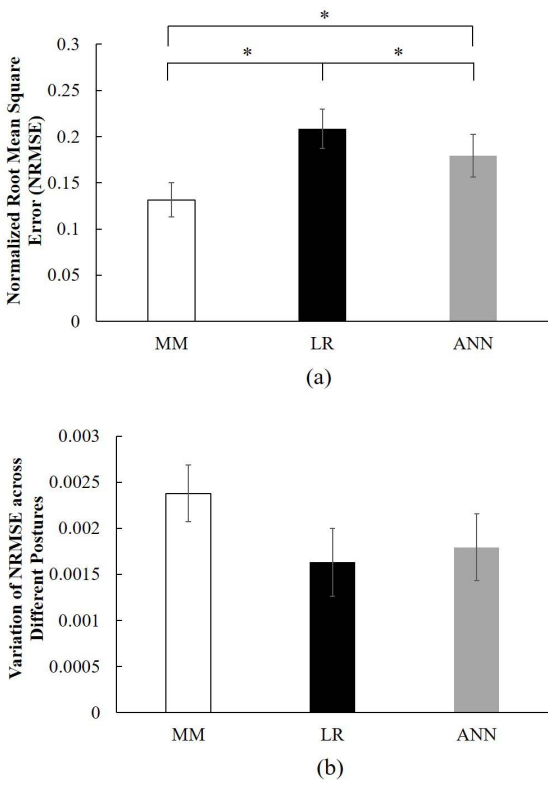

Fig. 5. (a) NRMSE between measured and estimated joint angles averaged across all AB subjects, movement types, joints, and postures for the test on MM (white bar), LR (black bar), and ANN (gray bar). (b) Variation in NRMSE across different postures. Tests marked by * indicate significant differences between algorithm types. Error bars represent the standard error.

the independent variable. To satisfy the normality requirement, a Fisher's transformation was applied to the measured values. In all ANOVA tests, a full statistical model was generated first. If no significant interaction was detected, a reduced ANOVA model with only main effects was conducted. Whenever significance was detected for the main factors, a Tukey comparison was performed. For all tests, the significance level was set to $p = 0.05$.

III. Results

The r values of MM, LR, and ANN were 0.88, 0.63, and 0.70, respectively, when averaged across all AB subjects, movement types, joints, and postures (Fig. 4a). The two-way ANOVA on r values revealed no two-way interaction ($p = 0.209$). ANOVA with only main effects indicated all variables to be statistically significant ($p < 0.001$ for all studied variables). For the factor of algorithm type, Tukey comparison revealed that the r value of MM was significantly higher than that of LR ($p < 0.001$) and ANN ($p < 0.001$). It also revealed that the r value of ANN was significantly higher than that of LR ($p < 0.001$).

Fig. 4b shows the variation in r across different postures. The one-way ANOVA on the variation in r across different postures revealed a significant main effect of algorithm type ($p = 0.004$). Tukey comparison revealed that the variation in r of MM was significantly lower than that of LR ($p < 0.001$) and ANN ($p < 0.001$).

The NRMSE values of MM, LR, and ANN were 0.13, 0.21, and 0.18, respectively, when averaged across all AB subjects, movement types, joints, and postures (Fig. 5a). The two-way ANOVA on NRMSE revealed no two-way interaction ($p = 0.197$). ANOVA with only main effects indicated all variables to be statistically significant ($p < 0.001$ for all studied variables). For the factor of algorithm type, Tukey comparison revealed that the NRMSE of MM was significantly lower than that of LR ($p < 0.001$) and ANN ($p < 0.001$). It also revealed that the NRMSE of ANN was significantly lower than that of LR ($p < 0.001$).

Fig. 5b shows the variation in NRMSE across different postures. The one-way ANOVA on the variation in NRMSE across different postures revealed no significant main effect of algorithm type ($p = 0.281$).

All portions of the data sets for MM had r values over 0.2, while several portions of the data sets for LR and ANN were negative (Fig. 6). All portions of the data sets for MM had

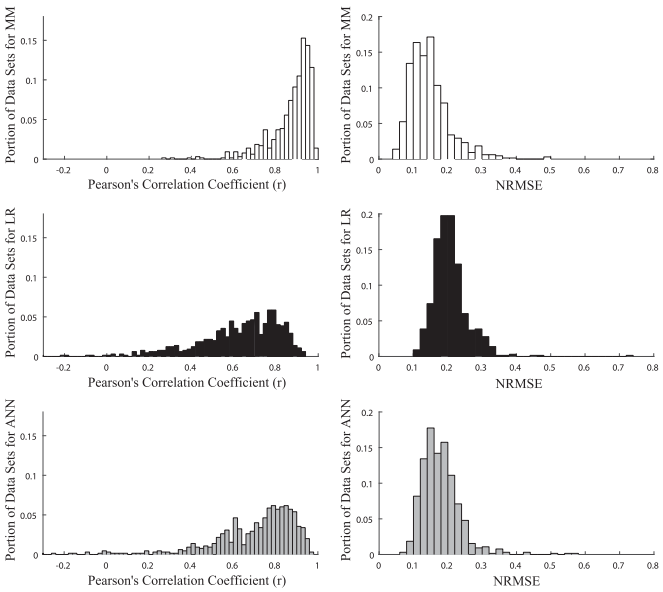

Fig. 6. Left side: histograms of the pearson's correlation coefficient (r) for the MM (white bar), LR (black bar), and ANN (gray bar). right side: histograms of the NRMSE for the MM (white bar), LR (black bar), and ANN (gray bar).

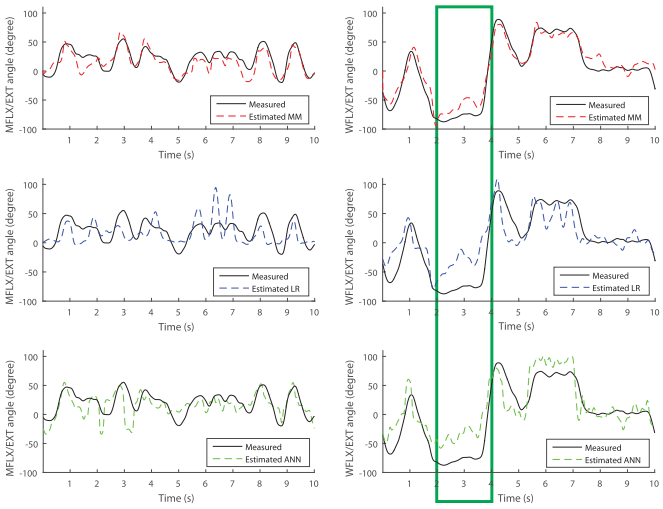

Fig. 7. Representative estimation performance during simultaneous 2-DoF random movements of the test on MM, LR, and ANN in the neutral posture P3 for AB subject 2. Measured joint angles are solid black lines. The estimated joint angles of MM, LR, and ANN are dashed red lines, blue lines, and green lines, respectively.

NRMSE values below 0.5, while several portions of the data sets for LR and ANN were over 0.5 (Fig. 6).

The estimated and measured joint angles for an exemplary trial of simultaneous 2-DoF random movement in neutral posture P3 for AB subject 2 are shown in Fig. 7. Qualitatively, the MM attained the best estimation performance (both waveform and magnitude) among all three algorithms (MM, LR, and ANN). There were instances when the LR estimated MCP movement that was much larger than the measured MCP movement, which could explain why the LR had the largest NRMSE among the three algorithms.

To better demonstrate the science/principle of the MM for EMG interface design, we investigated the biological processes from the muscle activations to the joint angles of the MM. Fig. 8 shows an example of the biological processes during simultaneous 2-DoF random movements in the neutral posture P3 for AB subject 2. Particularly at the WFLX/EXT DoF from 2 to 4 seconds, the MM predicted the joint angles much closer to the measured joint angles than the LR and ANN in Fig. 7. The active force of the muscle ECRL and the passive force of the muscle FCR counteracted to generate the joint moment at the WFLX/EXT DoF around 0 Nm and ensured the joint angle held at -80 degrees consistently. However, the LR and ANN did not account for those biological processes from the muscle activations to the joint angles and therefore could not capture the passive force that plays an important role in generating human motions from muscle activations.

For the amputee subject, we compared r value and NRMSE, averaged across all movement types, joints, and postures, derived from the test on MM, LR, and ANN, respectively. The average r values of the MM, LR, and ANN were 0.80, 062, and 0.57, respectively (Fig. 9a). The average NRMSE values of the test on MM, LR, and ANN were 0.15, 0.22, and 0.23, respectively (Fig. 9b). Qualitatively, the MM attained the best estimation performance (both waveform and magnitude) among all three algorithms (Fig. 10), just as we observed for the AB subjects.

IV. Discussion

In the present study, we compared the movement estimation performance of three algorithms used for EMG-based HMIs: MM, LR, and ANN. Overall, the MM could predict the trend (as indicated by r values) and magnitude (as indicated by NRMSE) of movements significantly better across the tested postures than either LR or ANN. The results were similar for both AB subjects and the amputee subject. Additionally, the variation in r across different postures of MM was significantly lower than that of either LR or ANN, indicating that the MM could estimate movement more reliably across postures than either LR or ANN.

Compared to LR and ANN, the better performance and higher reliability of the MM across different upper limb postures was potentially caused by the following characteristics: 1. The MM generally reflected the anatomical and physiological constraints of the neural, muscular, and skeletal systems of the wrist and hand, though in a simplified form. Since the musculoskeletal structure in both the human and model were fixed, the primary biomechanical actions of the muscles crossing the fingers and wrist were likely preserved across different upper limb postures. 2. Each EMG was measured primarily from one muscle and applied to a virtual muscle with comparable biomechanical behavior; thus, the output movements with activation of the biological and virtual muscles would generally match. 3. The MM accounted for the biological processes from the muscle activations to the joint angles and could capture the passive force, which was important to balance the active force while the subject held a joint at the position far from the neutral position (see Fig. 8). However, the data-driven approaches compared in this study (LR and ANN) were modeled based on the structure of the training data without

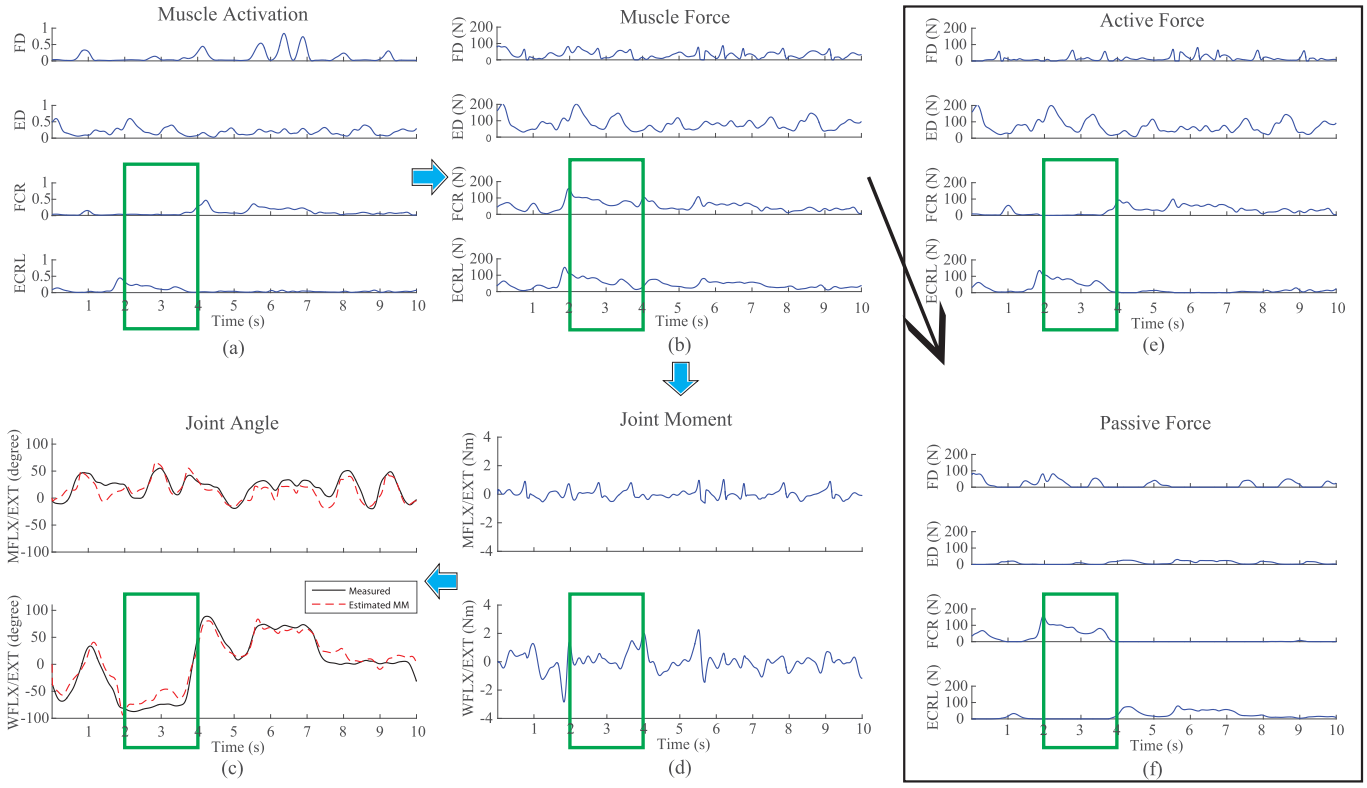

Fig. 8. Biological processes from the muscle activations to the joint angles of the MM during simultaneous 2-DoF random movements in the neutral posture P3 for AB subject 2. (a) Muscle activations of the four muscles; (b) Muscle forces of the four muscles; (c) Joint moments at the two joints; (d) Joint angles at the joints (measured joint angles are solid black lines and estimated joint angles are dashed red lines); (e) Active forces of the four muscles; (f) Passive forces of the four muscles.

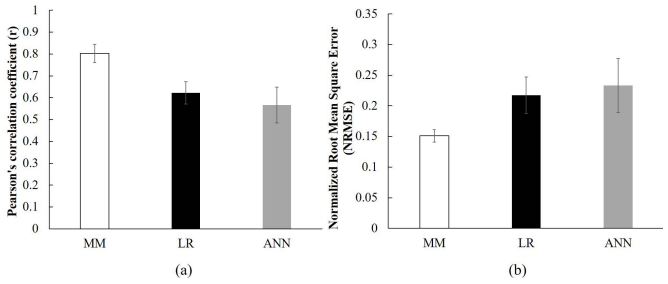

Fig. 9. (a) Comparison of the Pearson's correlation coefficient derived from the test on MM (white bar), LR (black bar), and ANN (gray bar); (b) Comparison of the NRMSE derived from the test on MM (white bar), LR (black bar), and ANN (gray bar). Error bars represent the standard error.

accounting for anatomical and physiological constraints and therefore cannot capture the passive force.

The estimation performance (r value and NRMSE) of both the MM and ANN was significantly better than that of LR for AB subjects. We attributed this to the fact that the neuromuscular system of the hand is a nonlinear system and, thus, difficult to characterize well with a linear model. Conversely, the nonlinear MM and ANN algorithms likely had better capability to characterize the nonlinear features of the neuromuscular system of the hand. It was interesting that the variation in r across different postures was significantly higher (worse) with ANN than with LR, even though the estimation performance was better (higher r value and lower NRMSE) with ANN than with LR. In other words, ANN was more accurate but less consistent across postures than LR. We attributed this to the fact that since ANN was a nonlinear algorithm and LR was a linear algorithm, ANN likely overfit the training data set in the neutral posture and could not be generalized to the other postures as accurately as LR.

The r value of the MM was over 0.83 in all tested postures for AB subjects, indicating that the MM could estimate the trend of the wrist and hand movements (i.e., waveform) very well across the nine different tested postures. However, the NRMSE of the MM was over 0.1 in the nine different postures, indicating that the MM could not estimate the magnitude as well as it could estimate the trend of the wrist and hand movements. Nevertheless, matching the measured joint motion exactly (both waveform and magnitude) is very likely not necessary for EMG-based HMIs. This is because (1) engineers can modify the control gain in EMG-based HMIs to better match the magnitude of joint motion, and (2) human users are adaptive and can adjust the EMG activation level volitionally to produce the desired magnitude of joint motion, given that the MM can predict the waveform fairly accurately.

Several studies suggested that human adaptation would be helpful to ensure the high performance of continuous EMG HMIs for real-time control [38], [40], [41]. Other study demonstrated that offline estimation performance has poor correlation with online, real-time control performance of continuous EMG HMIs [51]. We agree that, with the human in the loop during real-time continuous myoelectric

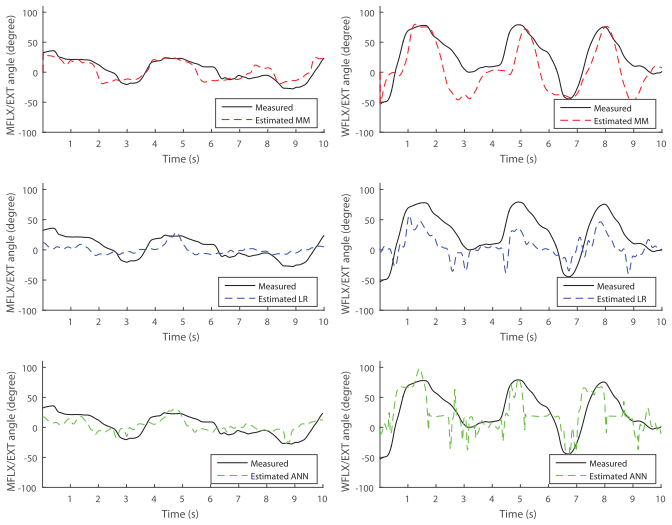

Fig. 10. Representative estimation performance during simultaneous 2-DoF random movements of the test on MM, LR, and ANN in the neutral posture P3 for the amputee subject. Measured joint angles are solid black lines. The estimated joint angles of MM, LR, and ANN are dashed red lines, blue lines, and green lines, respectively.

control, the human's adaptability could compensate to achieve good online performance with different control algorithms, even those with relatively poor offline performance. However, typical outcome metrics used in real-time myoelectric control studies do not sufficiently capture human adaptation effort (i.e., cognitive load and training time) to evaluate its contribution to control performance. Based on our offline comparison between the MM and data-driven approaches, we propose that accounting for anatomical musculoskeletal structure when developing continuous EMG interfaces could improve estimation performance. The better offline estimation performance of the MM may decrease the required human adaptation effort to ensure good real-time control performance.

There were several limitations of the current study. We compared the MM with only two representative data-driven algorithms that are widely used for EMG HMI. In future work, more data-driven algorithms should be considered. We tested one amputee subject to demonstrate the potential application of the MM for multifunctional prosthesis control. Recent studies [43], [45], [47] have shown that EMG-driven MM is a potentially viable method for prosthetic control in individuals with upper limb amputations since it is likely that the internal representation of MM of their missing limbs still exist. In this study we found that even for this amputee subject, the MM predicted movements more accurately than either LR or ANN. It would be an interesting future study to test more amputee subjects with MM-based neural interface in order to investigate the underneath mechanism and neural representation of missing limbs in individuals with limb losses. This future study might also inform the further design of MM-based neural interface tailored to amputee population for improved performance. Another limitation is that the amputee subject completed the testing in only 3 of the 9 upper limb postures to avoid fatigue. Appropriately planned resting time should be given to amputee subjects to ensure completing the testing in all 9 upper limb postures in the future.

Identifying EMG signals from specific muscles is necessary for the MM-based interface. To ensure that we could record muscle-specific EMG from the amputee subject, we used fine-wire electrodes. Fine-wire electrodes are suitable for lab testing, but not for daily practice. Recently, implantable myoelectric sensors (IMES) have been developed and evaluated in humans [64]. IMES could be a potential solution for the clinical application of MM for prosthesis control in the future. In addition to IMES, high-density (HD) EMG electrodes, which can obtain spatially more specific information, can be an alternative technique that does not require invasive recordings. We will use HD EMG recordings and existing source separation methods to locate specific muscles and EMG recording sites on the amputee's residual limb.

Our study showed the relatively superior estimation performance of MM for only 2 DoFs. An advantage of the regression learning approaches is that they can easily be extended to more DoFs. However, DoFs can also be added to the MM, as we previously demonstrated by adding wrist supination/pronation to the 2-DoF MM to construct a 3-DoF MM [65]. An important open question is whether the superior estimation performance of the MM would be preserved for >2 DoFs. To address this question in future work, we will compare the 3-DoF MM with the data-driven approaches in offline and real-time experiments.

V. Conclusion

Our study preliminarily compared estimation performance among three algorithms used for EMG-based HMIs: MM, LR, and ANN. Performance was evaluated for a variety of challenging movement conditions involving independent and simultaneous wrist and MCP joint movements across nine upper limb postures, which reflected the movements required to perform daily living tasks. Our results demonstrated that the MM, which directly incorporates knowledge about musculoskeletal structure and biological movement production, could estimate the trend (as indicated by r value) and magnitude (as indicated by NRMSE) of AB movements significantly better than either LR or ANN. Similar results were observed in the amputee subject. The results also indicated that the MM was more robust across different upper limb postures than either LR or ANN. Thus, incorporating neurophysiological knowledge into EMG-based HMIs may help improve the estimation of continuous, coordinated motion.

Acknowledgment

The authors thank all the subjects for taking part in the experiments.

References

[1] D. Graupe and W. K. Cline, "Functional separation of EMG signals via ARMA identification methods for prosthesis control purposes," *IEEE Trans. Syst. Man Cybern.*, vol. SMC-5, no. 2, pp. 252–259, Mar. 1975.

[2] P. C. Doerschuk, D. E. Gustafon, and A. S. Willsky, "Upper extremity limb function discrimination using EMG signal analysis," *IEEE Trans. Biomed. Eng.*, vol. BME-30, no. 1, pp. 18–29, Jan. 1983.

[3] A. Fougner, Ø. Stavdahl, P. J. Kyberd, Y. G. Losier, and P. Parker, "Control of upper limb prostheses: Terminology and proportional myoelectric control—A review," *IEEE Trans. Neural Syst. Rehabil. Eng.*, vol. 20, no. 5, pp. 663–677, Sep. 2012.

[4] D. Farina *et al.*, "The extraction of neural information from the surface EMG for the control of upper-limb prostheses: Emerging avenues and challenges," *IEEE Trans. Neural Syst. Rehabil. Eng.*, vol. 22, no. 4, pp. 797–809, Jul. 2014.

[5] M. Ortiz-Catalan, "Neuroengineering: Deciphering neural drive," *Nature Biomed. Eng.*, vol. 1, no. 2, 2017, Art. no. 0034.

[6] L. Liu, X. Chen, Z. Lu, S. Cao, D. Wu, and X. Zhang, "Development of an EMG-ACC-based upper limb rehabilitation training system," *IEEE Trans. Neural Syst. Rehabil. Eng.*, vol. 25, no. 3, pp. 244–253, Mar. 2017.

[7] M. Ortiz-Catalan, N. Sander, M. B. Kristoffersen, B. Håkansson, and R. Brånemark, "Treatment of phantom limb pain (PLP) based on augmented reality and gaming controlled by myoelectric pattern recognition: A case study of a chronic PLP patient," *Frontiers Neurosci.*, vol. 8, p. 24, Feb. 2014.

[8] L. Van Dijk, C. K. van der Sluis, H. W. van Dijk, and R. M. Bongers, "Task-oriented gaming for transfer to prosthesis use," *IEEE Trans. Neural Syst. Rehabil. Eng.*, vol. 24, no. 12, pp. 1384–1394, Dec. 2016.

[9] ThalmicLabs. (2016). *Myo Armband*. Accessed: Feb. 3, 2018. [Online]. Available: https://www.myo.com/

[10] J. W. L. Pau, S. S. Q. Xie, and A. J. Pullan, "Neuromuscular interfacing: Establishing an EMG-driven model for the human elbow joint," *IEEE Trans. Biomed. Eng.*, vol. 59, no. 9, pp. 2586–2593, Sep. 2012.

[11] D. Leonardis *et al.*, "An EMG-controlled robotic hand exoskeleton for bilateral rehabilitation," *IEEE Trans. Haptics*, vol. 8, no. 2, pp. 140–151, Jun. 2015.

[12] Y.-J. Kim, C.-K. Park, and K. G. Kim, "An EMG-based variable impedance control for elbow exercise: Preliminary study," *Adv. Robot.*, vol. 31, no. 15, pp. 809–820, 2017.

[13] Z. Li, D. Guiraud, D. Andreu, M. Benoussaad, C. Fattal, and M. Hayashibe, "Real-time estimation of FES-induced joint torque with evoked EMG," *J. Neuroeng. Rehabil.*, vol. 13, no. 1, 2016, Art. no. 60.

[14] K. B. Wilkins, M. Owen, C. Ingo, C. Carmona, J. P. A. Dewald, and J. Yao, "Neural plasticity in moderate to severe chronic stroke following a device-assisted task-specific arm/hand intervention," *Frontiers Neurol.*, vol. 8, p. 284, Jun. 2017.

[15] J. Jonsdottir *et al.*, "Arm rehabilitation in post stroke subjects: A randomized controlled trial on the efficacy of myoelectrically driven FES applied in a task-oriented approach," *PLoS ONE*, vol. 12, no. 12, 2017, Art. no. e0188642.

[16] P. K. Artemiadis and K. J. Kyriakopoulos, "EMG-based control of a robot arm using low-dimensional embeddings," *IEEE Trans. Robot.*, vol. 26, no. 2, pp. 393–398, Apr. 2010.

[17] P. K. Artemiadis and K. J. Kyriakopoulos, "A switching regime model for the EMG-based control of a robot arm," *IEEE Trans. Syst., Man, Cybern. B, Cybern.*, vol. 41, no. 1, pp. 53–63, Feb. 2011.

[18] J. Vogel, C. Castellini, and P. van der Smagt, "EMG-based teleoperation and manipulation with the DLR LWR-III," in *Proc. IEEE/RSJ Int. Conf. Intell. Robots Syst. (IROS)*, Sep. 2011, pp. 672–678.

[19] K. Østlie, I. M. Lesjø, R. J. Franklin, B. Garfelt, O. H. Skjeldal, and P. Magnus, "Prosthesis rejection in acquired major upper-limb amputees: A population-based survey," *Disab. Rehabil. Assist. Technol.*, vol. 7, no. 4, pp. 294–303, 2012.

[20] J. Davidson, "A survey of the satisfaction of upper limb amputees with their prostheses, their lifestyles, and their abilities," *J. Hand Therapy*, vol. 15, no. 1, pp. 62–70, 2002.

[21] B. Hudgins, P. Parker, and R. N. Scott, "A new strategy for multifunction myoelectric control," *IEEE Trans. Biomed. Eng.*, vol. 40, no. 1, pp. 82–94, Jan. 1993.

[22] K. Englehart and B. Hudgins, "A robust, real-time control scheme for multifunction myoelectric control," *IEEE Trans. Biomed. Eng.*, vol. 50, no. 7, pp. 848–854, Jul. 2003.

[23] H. Huang, P. Zhou, G. Li, and T. Kuiken, "Spatial filtering improves EMG classification accuracy following targeted muscle reinnervation," *Ann. Biomed. Eng.*, vol. 37, no. 9, pp. 1849–1857, 2009.

[24] L. Pan, D. Zhang, N. Jiang, X. Sheng, and X. Zhu, "Improving robustness against electrode shift of high density EMG for myoelectric control through common spatial patterns," *J. Neuroeng. Rehabil.*, vol. 12, no. 1, p. 110, 2015.

[25] X. Zhang and H. Huang, "A real-time, practical sensor fault-tolerant module for robust EMG pattern recognition," *J. Neuroeng. Rehabil.*, vol. 12, no. 1, 2015, Art. no. 18.

[26] A. A. Adewuyi, L. J. Hargrove, and T. A. Kuiken, "An analysis of intrinsic and extrinsic hand muscle EMG for improved pattern recognition control," *IEEE Trans. Neural Syst. Rehabil. Eng.*, vol. 24, no. 4, pp. 485–494, Apr. 2015.

[27] R. B. Woodward and L. J. Hargrove, "Adapting myoelectric control in real-time using a virtual environment," *J. Neuroeng. Rehabil.*, vol. 16, no. 1, 2019, Art. no. 11.

[28] J. Robertson, E. Scheme, and K. Englehart, "Effects of confidence-based rejection on usability and error in pattern recognition-based myoelectric control," *IEEE J. Biomed. Health Inform.*, to be published.

[29] A. Waris, I. K. Niazi, M. Jamil, K. Englehart, W. Jensen, and E. N. Kamavuako, "Multiday evaluation of techniques for EMG-based classification of hand motions," *IEEE J. Biomed. Health Inform.*, vol. 23, no. 4, pp. 1526–1534, Jul. 2019.

[30] J. Maier, A. Naber, and M. Ortiz-Catalan, "Improved prosthetic control based on myoelectric pattern recognition via wavelet-based de-noising," *IEEE Trans. Neural Syst. Rehabil. Eng.*, vol. 26, no. 2, pp. 506–514, Feb. 2017.

[31] M. Ortiz-Catalan, B. Håkansson, and R. Brånemark, "An osseointegrated human-machine gateway for long-term sensory feedback and motor control of artificial limbs," *Sci. Transl. Med.*, vol. 6, no. 257, p. 257re6, Oct. 2014.

[32] M. Ortiz-Catalan, B. Håkansson, and R. Brånemark, "Real-time and simultaneous control of artificial limbs based on pattern recognition algorithms," *IEEE Trans. Neural Syst. Rehabil. Eng.*, vol. 22, no. 4, pp. 756–764, Jul. 2014.

[33] J. L. Nielsen, S. Holmgaard, N. Jiang, K. B. Englehart, D. Farina, and P. A. Parker, "Simultaneous and proportional force estimation for multifunction myoelectric prostheses using mirrored bilateral training," *IEEE Trans. Biomed. Eng.*, vol. 58, no. 3, pp. 681–688, Mar. 2011.

[34] N. Jiang, K. B. Englehart, and P. A. Parker, "Extracting simultaneous and proportional neural control information for multiple-DOF prostheses from the surface electromyographic signal," *IEEE Trans. Biomed. Eng.*, vol. 56, no. 4, pp. 1070–1080, Apr. 2009.

[35] N. Jiang, J. Nielsen, S. Muceli, and D. Farina, "EMG-based simultaneous and proportional estimation of wrist kinematics and its application in intuitive myoelectric control for unilateral transradial amputees," in *Proc. Front. Comput. Neurosci. Conf. Abstract, BC11, Comput. Neurosci. Neurotechnol. Bernstein Conf. Neurex Annu. Meeting*, 2011.

[36] S. Muceli and D. Farina, "Simultaneous and proportional estimation of hand kinematics from EMG during mirrored movements at multiple degrees-of-freedom," *IEEE Trans. Neural Syst. Rehabil. Eng.*, vol. 20, no. 3, pp. 371–378, May 2012.

[37] N. Jiang, H. Rehbaum, I. Vujaklija, B. Graimann, and D. Farina, "Intuitive, online, simultaneous, and proportional myoelectric control over two degrees-of-freedom in upper limb amputees," *IEEE Trans. Neural Syst. Rehabil. Eng.*, vol. 22, no. 3, pp. 501–510, May 2014.

[38] J. M. Hahne *et al.*, "Linear and nonlinear regression techniques for simultaneous and proportional myoelectric control," *IEEE Trans. Neural Syst. Rehabil. Eng.*, vol. 22, no. 2, pp. 269–279, Mar. 2014.

[39] L. H. Smith, T. A. Kuiken, and L. J. Hargrove, "Evaluation of linear regression simultaneous myoelectric control using intramuscular EMG," *IEEE Trans. Biomed. Eng.*, vol. 63, no. 4, pp. 737–746, Apr. 2016.

[40] S. Amsuess *et al.*, "Context-dependent upper limb prosthesis control for natural and robust use," *IEEE Trans. Neural Syst. Rehabil. Eng.*, vol. 24, no. 7, pp. 744–753, Jul. 2016.

[41] J. M. Hahne, M. Markovic, and D. Farina, "User adaptation in myoelectric man-machine interfaces," *Sci. Rep.*, vol. 7, no. 1, 2017, Art. no. 4437.

[42] D. Blana, J. G. Hincapie, E. K. Chadwick, and R. F. Kirsch, "A musculoskeletal model of the upper extremity for use in the development of neuroprosthetic systems," *J. Biomech.*, vol. 41, no. 8, pp. 1714–1721, 2008.

[43] D. Blana, E. K. Chadwick, A. J. van den Bogert, and W. M. Murray, "Real-time simulation of hand motion for prosthesis control," *Comput. Methods Biomech. Biomed. Eng.*, vol. 20, no. 5, pp. 540–549, 2017.

[44] E. K. Chadwick, D. Blana, A. J. van den Bogert, and R. F. Kirsch, "A real-time, 3-D musculoskeletal model for dynamic simulation of arm movements," *IEEE Trans. Biomed. Eng.*, vol. 56, no. 4, pp. 941–948, Apr. 2009.

[45] D. L. Crouch and H. Huang, "Lumped-parameter electromyogram-driven musculoskeletal hand model: A potential platform for real-time prosthesis control," *J. Biomech.*, vol. 49, no. 16, pp. 3901–3907, 2016.

[46] M. Sartori, D. G. Llyod, and D. Farina, "Neural data-driven musculoskeletal modeling for personalized neurorehabilitation technologies," *IEEE Trans. Biomed. Eng.*, vol. 63, no. 5, pp. 879–893, May 2016.

[47] M. Sartori, G. Durandau, S. Došen, and D. Farina, "Robust simultaneous myoelectric control of multiple degrees of freedom in wrist-hand prostheses by real-time neuromusculoskeletal modeling," *J. Neural Eng.*, vol. 15, no. 6, 2018, Art. no. 066026.

[48] L. Pan, D. L. Crouch, and H. Huang, "Myoelectric control based on a generic musculoskeletal model: Toward a multi-user neural-machine interface," *IEEE Trans. Neural Syst. Rehabil. Eng.*, vol. 26, no. 7, pp. 1435–1442, Jul. 2018.

[49] D. L. Crouch and H. Huang, "Musculoskeletal model predicts multi-joint wrist and hand movement from limited EMG control signals," in *Proc. 37th Annu. Int. Conf. IEEE Eng. Med. Biol. Soc. (EMBC)*, Aug. 2015, pp. 1132–1135.

[50] D. L. Crouch and H. Huang, "Musculoskeletal model-based control interface mimics physiologic hand dynamics during path tracing task," *J. Neural Eng.*, vol. 14, no. 3, 2017, Art. no. 036008.

[51] N. Jiang, I. Vujaklija, H. Rehbaum, B. Graimann, and D. Farina, "Is accurate mapping of EMG signals on kinematics needed for precise online myoelectric control?" *IEEE Trans. Neural Syst. Rehabil. Eng.*, vol. 22, no. 3, pp. 549–558, May 2014.

[52] A. Fougner, E. Scheme, A. D. C. Chan, K. Englehart, and Ø. Stavdahl, "Resolving the limb position effect in myoelectric pattern recognition," *IEEE Trans. Neural Syst. Rehabil. Eng.*, vol. 19, no. 6, pp. 644–651, Dec. 2011.

[53] Y. Geng, P. Zhou, and G. Li, "Toward attenuating the impact of arm positions on electromyography pattern-recognition based motion classification in transradial amputees," *J. Neuroeng. Rehabil.*, vol. 9, no. 1, 2012, Art. no. 74.

[54] N. Jiang, S. Muceli, B. Graimann, and D. Farina, "Effect of arm position on the prediction of kinematics from EMG in amputees," *Med. Biol. Eng. Comput.*, vol. 51, nos. 1–2, pp. 143–151, 2013.

[55] J. Liu, D. Zhang, X. Sheng, and X. Zhu, "Quantification and solutions of arm movements effect on sEMG pattern recognition," *Biomed. Signal Process. Control*, vol. 13, pp. 189–197, Sep. 2014.

[56] D. Yang, Y. Gu, L. Jiang, L. Osborn, and H. Liu, "Dynamic training protocol improves the robustness of PR-based myoelectric control," *Biomed. Signal Process. Control*, vol. 31, pp. 249–256, Jan. 2017.

[57] Y. Geng, O. W. Samuel, Y. Wei, and G. Li, "Improving the robustness of real-time myoelectric pattern recognition against arm position changes in transradial amputees," *BioMed Res. Int.*, vol. 2017, Apr. 2017, Art. no. 5090454.

[58] J. Cheng, F. Wei, C. Li, Y. Liu, A. Liu, and X. Chen, "Position-independent gesture recognition using sEMG signals via canonical correlation analysis," *Comput. Biol. Med.*, vol. 103, pp. 44–54, Dec. 2018.

[59] I. Kyranou, S. Vijayakumar, and M. S. Erden, "Causes of performance degradation in non-invasive electromyographic pattern recognition in upper limb prostheses," *Frontiers Neurorobot.*, vol. 12, Sep. 2018, Art. no. 58.

[60] K. R. S. Holzbaur, W. M. Murray, and S. L. Delp, "A model of the upper extremity for simulating musculoskeletal surgery and analyzing neuromuscular control," *Ann. Biomed. Eng.*, vol. 33, no. 6, pp. 829–840, 2005.

[61] D. G. Lloyd and T. F. Besier, "An EMG-driven musculoskeletal model to estimate muscle forces and knee joint moments *in vivo*," *J. Biomech.*, vol. 36, no. 6, pp. 765–776, 2003.

[62] R. Heine, K. Manal, and T. S. Buchanan, "Using Hill-type muscle models and EMG data in a forward dynamic analysis of joint moment: Evaluation of critical parameters," *J. Mech. Med. Biol.*, vol. 3, no. 2, pp. 169–186, 2003.

[63] J. M. Winters, "Hill-based muscle models: A systems engineering perspective," in *Multiple Muscle Systems*. New York, NY, USA: Springer, 1990, pp. 69–93.

[64] R. F. Weir, P. R. Troyk, G. A. DeMichele, D. A. Kerns, J. F. Schorsch, and H. Maas, "Implantable myoelectric sensors (IMESs) for intramuscular electromyogram recording," *IEEE Trans. Biomed. Eng.*, vol. 56, no. 1, pp. 159–171, Jan. 2009.

[65] L. Pan, D. Crouch, and H. Huang, "Musculoskeletal model for simultaneous and proportional control of 3-DOF hand and wrist movements from EMG signals," in *Proc. 8th Annu. Int. IEEE EMBS Conf. Neural Eng.*, May 2017, pp. 325–328.